New analytical ($^2A'$,$^4A'$) surfaces and theoretical rate constants for the N(^4S)+O_2 reaction

R. Sayós,[a] Carolina Oliva, and Miguel González[b]
Departament de Química Física i Centre de Recerca en Química Teòrica, Universitat de Barcelona, C/Martí i Franquès 1, 08028 Barcelona, Spain

(Received 31 January 2002; accepted 16 April 2002)

We report two new analytical fits of the ground potential energy surface (PES) ($^2A'$) and the first excited PES ($^4A'$) involved into the title reaction and its reverse, using *ab initio* electronic structure calculations from Papers I and II along with new grids of *ab initio* points by means of the second-order perturbation theory on CASSCF wave function [CASPT2 (17,12) G2/aug-cc-pVTZ] reported here (1250 points for the $^2A'$ PES and 910 points for the $^4A'$ PES). Some experimental data were also introduced to better account for the exoergicity and the experimental rate constant at 300 K. The final root-mean-square deviations of the fits were 1.06 and 1.67 kcal/mol for $^2A'$ and the $^4A'$ PESs, respectively, for the NOO C_s abstraction and insertion regions of the PESs. Thermal rate constants were calculated (300–5000 K) for both the direct and reverse reactions by means of the variational transition state theory with the inclusion of a microcanonical optimized multidimensional tunneling correction, obtaining a very good agreement with the experimental data within all the temperature range. The new analytical $^2A'$ PES presents several stationary points not introduced in previous analytical surfaces, and describes accurately the NO_2 ($X\,^2A_1$) minimum, which seems to be very accessible according to the trajectories run in a preliminary quasiclassical trajectory study. The new analytical $^4A'$ PES has a lower energy barrier than the previous one, which increases significantly the contribution of this PES to the total rate constant at high temperatures. Moreover, the new analytical PESs not only describe accurately the C_s regions of the NOO system but also the ONO C_{2v} or near C_{2v} regions. © *2002 American Institute of Physics.* [DOI: 10.1063/1.1483853]

I. INTRODUCTION

The elementary gas-phase reaction of nitrogen in its ground electronic state with molecular oxygen,

$$N(^4S)+O_2(X\,^3\Sigma_g^-)\rightarrow O(^3P)+NO(X\,^2\Pi), \qquad (1)$$

$$\Delta_r H^0_{0\ K}=-32.09\ \text{kcal/mol}$$

(Ref. 1) and its reverse reaction play an important role in the Earth's atmospheric chemistry. This reaction is a source of infrared chemiluminescence in the thermosphere.[2] N(^4S) translational energy distributions in the terrestrial thermosphere are highly nonthermal in the energy range from 0.2 to 2 eV.[3] Therefore, the measured or calculated thermal rate constants are not suitable to explain the NO production in the thermosphere. The kinetics of NO formation is also important in shock heated air, supersonic expansion of exhaust gases and combustion processes with hydrocarbon–air mixtures.[4] High temperature studies of the kinetics and dynamics of the N(^4S)+O_2 and N(^4S)+NO reactions and their reverse ones are also very important to understand the chemical and physical phenomena taking place during the re-entry of spacecrafts into the Earth's atmosphere,[5] where nonthermal equilibrium conditions between the different degrees of freedom may play an essential role.

There are some available experimental data about thermal rate constants and NO vibrational distributions. Two compilations of kinetic data cover a wide range of temperatures: $k=1.5\times10^{-11}e^{-3600/T}$ cm^3 molecule^{-1} s^{-1} at 280–910 K (Ref. 6) or $1.5\times10^{-14}\ Te^{-3270/T}$ cm^3 molecule^{-1} s^{-1} at 298–5000 K.[7] Measurements of NO vibrational distributions show a significant population for $v'=0-7$, but also present important differences on their shapes for reactants at room temperature.[8–11] Moreover, an unexpected oscillatory NO(v') distribution has been reported by only two studies at both room temperature[11] and at higher energies (i.e., N atom velocities of 8 km/s).[12]

Several *ab initio* studies have been reported about the ground ($^2A'$) and the first excited ($^4A'$) potential energy surfaces (PES) involved in this reaction. Thus, earlier complete active space self-consistent-field (CASSCF) and multireference contracted configuration interaction (MR–CI) calculations with large Gaussian basis sets[13] were carried out for both PESs aimed at characterizing the transition states and minimum energy reaction paths (MEP). The same *ab initio* method but with large ANO basis sets were also used in a more recent theoretical study of the ground $^2A'$ PES.[14] Two recent extensive *ab initio* studies of our research group have been made on both PESs by means of CASSCF,

[a]Author to whom correspondence should be addressed. Electronic mail: r.sayos@qf.ub.es
[b]Electronic mail: miguel@qf.ub.es

second-order perturbation theory over the CASSCF wave function (CASPT2) and MR–CI calculations, and also some density functional calculations (B3LYP functional) with standard correlation-consistent Dunning basis sets and atomic natural orbital basis sets. In the first one[15] (hereafter referred to as Paper I), accurate energy barriers for both PESs were obtained and it was concluded that a peroxy NOO minimum might play an important role in the opening of two competitive microscopic reaction mechanisms: direct C_s abstraction versus indirect C_s insertion through the minimum corresponding to the NO_2 ($X\,^2A_1$) molecule. In the second *ab initio* study[16] (Paper II), the lowest A_1, B_1, A_2, and B_2 doublet and quartet PESs were characterized along with the location of several surface crossings. High-energy barriers were found for a direct C_{2v}-insertion mechanism, clearly showing that this microscopic competitive mechanism was much less favorable than the direct C_s-abstraction or the indirect C_s-insertion reaction mechanisms reported in Paper I.

Several analytical fits of the lowest doublet PES have been reported in previous works based mainly on *ab initio* data of Ref. 13. Most of them[17,18] are also based on the analytical form (many-body expansion) and parameters (diatomic terms and reference structure of the three-body term) introduced by our own.[19] Two earlier analytical $^2A'$ PESs, one of bond-order type derived from *ab initio* data,[14] and another of double many body form based on diatomics-in-molecules (DIM) and *ab initio* data,[20] are available in the literature, although they do not reproduce properly neither the *ab initio* information nor the known kinetic experimental data. For the quartet PES, only one analytical surface has been developed, using a similar procedure than that for the ground $^2A'$ PES.[18] Quasiclassical trajectory (QCT) studies,[18,19,21–25] variational transition state theory (VTST) studies[14,17] and quantum studies[26–28] have also been performed to study the kinetics and dynamics of the reaction (1) by using the mentioned PESs.

In the present work we have constructed analytical PESs for both $^2A'$ and $^4A'$ states based on the accurate *ab initio* data published in Papers I and II along with new extra grids of *ab initio* points here reported. Our hope is that these new PESs will furnish better kinetic and dynamical data, and also will allow a deeper comprehension of the yield of the several microscopic mechanisms involved in the title reaction.

This paper is organized as follows: the *ab initio* method and the fit procedure are described in Sec. II, several variational transition state theory calculations on thermal rate constants are presented in Sec. III, and finally Sec. IV shows the main concluding remarks.

II. ANALYTICAL POTENTIAL ENERGY SURFACES

A. *Ab initio* quantum chemical and surface fitting methods

The additional *ab initio* quantum chemical calculations to the previous published information[15,16] necessary to build the analytical PESs have been performed using the same method as in Papers I and II. Thus, the CASSCF method[29,30] was used throughout this study, always choosing the lowest two roots in C_s symmetry for both the doublet and the quarter PESs (i.e., A' and A''), which were obtained using the two-state-averaged method.[31] The full-valence active space comprising 17 electrons in 12 orbitals [i.e., CAS(17, 12)] was applied in all calculations as in previous papers. The standard correlation-consistent aug-cc-pVTZ basis set[32] was also used in the present study (138 basis functions, 46 on each atom). The dynamical correlation energy was included by performing CASPT2 calculations using the G2 variant;[33] all calculations were done with the MOLCAS 4.1 program.[34]

A many-body expansion[35] has been employed to derive an analytical expression for both the $^2A'$ and the $^4A'$ NOO potential energy surfaces. In both cases this expansion can be written as

$$V(R_1,R_2,R_3)=V^{(2)}_{\mathrm{NO}}(R_1)+V^{(2)}_{\mathrm{OO'}}(R_2)+V^{(2)}_{\mathrm{NO'}}(R_3)+V^{(3)}_{\mathrm{NOO'}}(R_1,R_2,R_3), \tag{2}$$

where $V^{(2)}$ and $V^{(3)}$ are the two- and three-body terms, respectively, and R_1, R_2, and R_3 are the NO, OO′, and NO′ distances, respectively. The one-body $V^{(1)}$ terms have been omitted because for all dissociation channels the atoms are in their ground electronic states: $N(^4S)+O(^3P)+O'(^3P)$. The two-body terms (diatomic potential energy curves) have been fitted using an extended-Rydberg potential up to third or fifth order,

$$V^{(2)}(R)=-D_e\left(1+\sum_{i=1}^{n\leqslant 5} a_i\rho^i\right)e^{-a_1\rho}, \tag{3}$$

where D_e and R_e are the dissociation energy and the equilibrium bond length of the corresponding diatomic molecule, respectively, and ρ is defined as $R-R_e$.

The three-body term consists of a product of a seventh-order polynomial $P(S_1,S_2,S_3)$ and a range function $T(S_1,S_2,S_3)$, both expressed in terms of symmetry-adapted coordinates (S_1,S_2,S_3):

$$V^{(3)}_{\mathrm{NOO'}}(S_1,S_2,S_3)=P(S_1,S_2,S_3)\cdot T(S_1,S_2,S_3) \tag{4}$$

with

$$P(S_1,S_2,S_3)=\sum_{i,j,k=0}^{0\leqslant i+j+k\leqslant 7} c_{ijk}S_1^iS_2^jS_3^k \tag{5}$$

with i, j, and k being positive integer numbers, and

$$T(S_1,S_2,S_3)=\prod_{i=1}^{3}\left[1-\tanh\left(\frac{\gamma_iS_i}{2}\right)\right]. \tag{6}$$

The range function tends to cancel the three-body term whenever one of the three atoms is separated from the other two. The symmetry-adapted coordinates are given by

$$S_1=\frac{1}{\sqrt{2}}(\rho_1+\rho_3),$$

$$S_2=\rho_2, \tag{7}$$

$$S_3=\frac{1}{\sqrt{2}}(\rho_1-\rho_3),$$

TABLE I. Optimal parameters for the $^2A'$ and $^4A'$ analytical PESs.

Two-body terms[a] Species	a_1	a_2	a_3	a_4	a_5
$O_2(X\,^3\Sigma_g^-)$	5.9003	10.226	8.7805		
$NO(X\,^2\Pi)$	5.6151	8.5237	5.3658	−2.4153	1.6274

Three-body terms[b]	$^2A'$	$^4A'$		$^2A'$	$^4A'$		$^2A'$	$^4A'$
c_{000}	4.0055	3.8282	c_{230}	13.887	27.253	c_{520}	15.158	−14.499
c_{100}	1.4305	2.9856	c_{212}	51.734	−98.379	c_{502}	4.2657	11.750
c_{010}	3.1728	−2.9419	c_{140}	−10.895	23.281	c_{430}	73.214	89.684
c_{200}	6.1786	9.0470	c_{122}	−94.140	46.628	c_{412}	−16.514	−20.315
c_{110}	18.521	9.7621	c_{104}	−19.983	20.384	c_{340}	−217.23	−113.07
c_{020}	−10.599	−8.9770	c_{050}	19.997	−7.4577	c_{322}	114.51	−46.144
c_{002}	−3.6118	−2.3334	c_{032}	19.191	−18.466	c_{304}	14.637	−7.2602
c_{300}	5.7945	3.8236	c_{014}	9.4733	−20.229	c_{250}	104.45	43.601
c_{210}	18.172	−0.6432	c_{600}	−1.4557	0.2404	c_{232}	−100.86	73.053
c_{120}	19.982	−4.7829	c_{510}	−1.3280	9.8025	c_{214}	−148.55	29.386
c_{102}	10.497	−3.2610	c_{420}	50.126	−19.597	c_{160}	−71.163	−4.5249
c_{030}	−17.105	3.4153	c_{402}	1.3586	28.401	c_{142}	66.889	−23.088
c_{012}	−10.344	3.6031	c_{330}	190.81	169.22	c_{124}	90.976	−26.473
c_{400}	0.8297	3.2305	c_{312}	30.686	−109.11	c_{106}	16.120	−13.582
c_{310}	19.457	−10.161	c_{240}	−221.80	−112.20	c_{070}	28.996	−0.1967
c_{220}	121.66	64.663	c_{222}	−60.200	−43.236	c_{052}	0.3620	2.4702
c_{202}	−1.8370	−24.713	c_{204}	8.9939	63.015	c_{034}	−21.235	7.6061
c_{130}	−74.182	−38.133	c_{150}	117.21	11.356	c_{016}	−6.9901	6.1873
c_{112}	−31.483	−28.590	c_{132}	5.5430	15.953			
c_{040}	46.000	12.289	c_{114}	−0.4791	6.7206	γ_1	4.4602	4.8692
c_{022}	−1.2032	19.232	c_{060}	−68.244	1.7358	γ_2	3.3212	0.7210
c_{004}	4.9259	6.5426	c_{042}	−14.165	−5.7173			
c_{500}	−2.4334	3.0059	c_{024}	17.523	2.2813	R_1^0	1.8340	1.8204
c_{410}	21.949	8.3595	c_{006}	−1.8864	−2.3397	R_2^0	1.5655	1.5536
c_{320}	109.16	45.422	c_{700}	−0.4640	−1.0915			
c_{302}	10.877	4.8771	c_{610}	−6.7683	−0.4127	R_3^0	1.8340	1.8204

[a]The dissociation energies and the equilibrium distances used in the fit are given in Table II.
[b]Units are c_{ijk}/eV Å$^{-(i+j+k)}$, γ_i/Å^{-1}, R_i^0/Å, a_i/Å^{-i}, where $R_1=R_{NO}$, $R_2=R_{OO'}$, and $R_3=R_{NO'}$.

and $\rho_i=R_i-R_i^0$, with (R_1^0,R_2^0,R_3^0) being a reference C_{2v} structure. The use of these coordinates makes sure the permutational OO′ symmetry of the analytical PES.

The two-body parameters (a_i) were fitted by means of a nonlinear least-squares procedure[36] and the three-body parameters (c_{ijk} and γ_i) by a weighted or nonweighted nonlinear least-squares method,[37] in both cases with a similar strategy to that followed in previous works of our own [e.g., $N(^2D)+O_2$,[38] $N(^2D)+NO$,[39] and $H+ClF$[40] reactions].

B. $^2A'$ analytical PES

A total of 27 and 34 *ab initio* points [CASPT2 (17, 12) G2/aug-cc-pVTZ] have been calculated for the O_2 and NO diatomic molecules, respectively, and fitted by using an extended-Rydberg potential curve [Eq. (3)] up to third order for O_2 and up to fifth order for NO. The spectroscopic D_e value[41] was used for O_2 while the *ab initio* D_e value for NO was good enough to be used in the fit. The final root-mean-square deviation (RMSD) of the fit in each diatomic energy curve was 0.61 and 0.57 kcal/mol for O_2 and NO, respectively. The optimal parameters are shown in Table I. The analytical spectroscopic constants of the diatomic molecules derived from the optimal analytical curves are summarized in Table II, which compared very well with the experimental data. Figure 1 shows the optimal diatomic energy curves obtained.

TABLE II. Spectroscopic constants of the diatomic molecules.

Molecule	ω_e(cm^{-1})	$\omega_e x_e$(cm^{-1})	B_e(cm^{-1})	α_e(cm^{-1})	$\overline{D_e}$(cm^{-1})	D_e(kcal/mol)	R_e(Å)
$NO(X\,^2\Pi)$							
Analytical fit	1869.3	11.537	1.6820	1.4919×10^{-2}	5.4466×10^{-6}	152.78	1.1586
Experimental[a]	1904.2	14.075	1.6720	1.71×10^{-2}	5.47×10^{-6}	152.53	1.1508
$O_2(X\,^3\Sigma_g^-)$							
Analytical fit	1595.5	10.786	1.4456	1.4493×10^{-2}	4.7496×10^{-6}	120.22	1.2075
Experimental[a]	1580.2	11.981	1.4377	1.593×10^{-2}	4.839×10^{-6}	120.22	1.2075

[a]Reference 40.

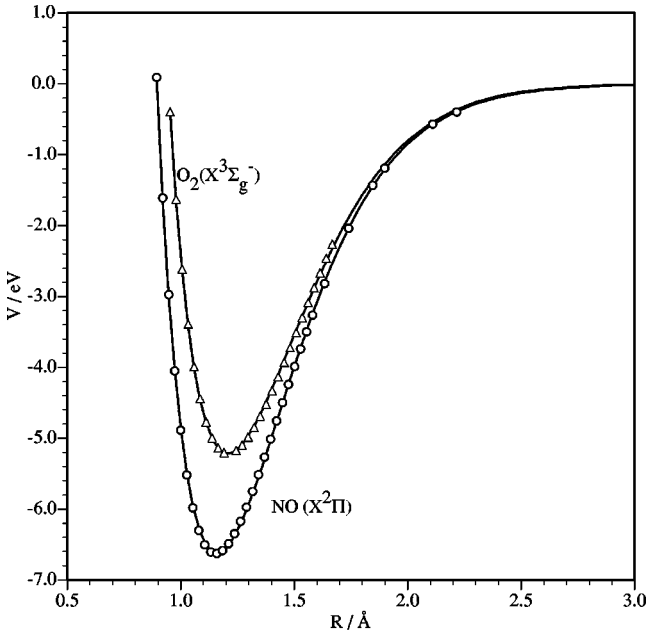

FIG. 1. *Ab initio* [CASPT2 (17,12) G2/aug-cc-pVTZ] diatomic points for the NO($X\ ^2\Pi$) and $O_2(X\ ^3\Sigma_g^-)$ molecules. Solid lines show an analytical fit which reproduces the experimental D_e.

A total of about 1250 *ab initio* points [CASPT2 (17,12) G2/aug-cc-pVTZ] have been computed in different regions of the $^2A'$ PES to be used in the analytical fit, as it is summarized below.

(a) 887 points for the $N(^4S)+O_2-C_s$-abstraction and insertion mechanisms: 681 points at different NOO angles (90°, 120°, 150°, and 180°) for 1.05 Å$\leqslant R_{NO} \leqslant$4.5 Å and 1.1 Å$\leqslant R_{OO} \leqslant$4.5 Å and 206 points around the transition states and minima (i.e., TS1, TS2, TS3, TS4, MIN1, and MIN2) involved in both mechanisms[15] (bending and stretching distortions), (b) 358 points for the $N(^4S)+O_2-C_{2v}$-insertion mechanism[16] for 0.0 Å$\leqslant R \leqslant$5.0 Å and 1.1 Å$\leqslant r \leqslant$2.6 Å, mainly around the $NO_2(X\ ^2A_1)$ minimum, where R is the N–O_2 (center of mass) distance and r the OO distance.

For the $^2A'$ surface it was not necessary to use the weighted nonlinear least-squares method (i.e., all points use a weight equal to 1) to obtain a good fit. Two minor corrections were introduced in the *ab initio* data that was used as input in the fit. First of all, the energy barrier corresponding to the TS1, the main transition state for this reaction, was slightly increased according to the results obtained in Paper I and the conclusions drawn in our previous PES.[17] In order to determine the optimal scale factor we made a first run of variational transition state calculations[42] on the thermal rate constant at 300 K to match the experimental value. Thus, 141 *ab initio* points along the intrinsic reaction coordinate (IRC) of the TS1 with a scale factor of 1.25 were introduced in the fit (with a weight of 1.0) to increase the energy barrier to approximately 6.9 kcal/mol. This final energy barrier was somewhat higher than the previous one used by us[17] (6.18 kcal/mol), but it was lower than that reported in previous analytical PESs (e.g., 7.03[18] or 7.54[19] kcal/mol). Second, the *ab initio* points in the entrance channel [i.e., $N(^4S)+O_2$] were shifted by summing up 5.73 kcal/mol to reproduce the experimental exoergicity, as the *ab initio* dissociation energy for O_2 molecule was not accurate enough.

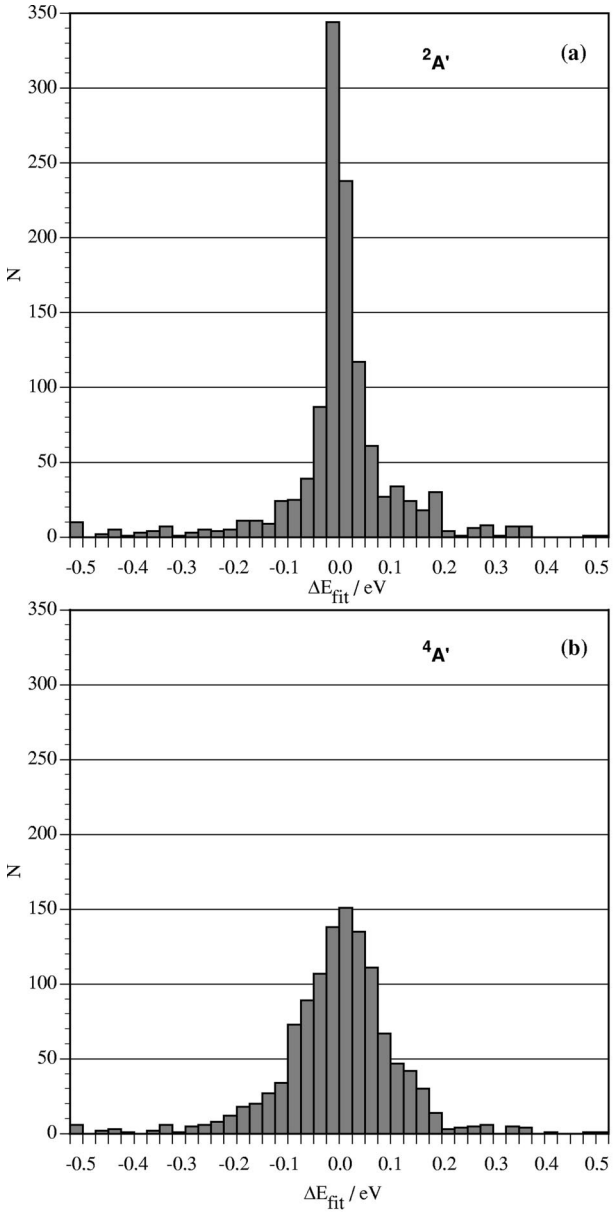

FIG. 2. Distribution of the energy deviations (i.e., $\Delta E = E_{analytical} - E_{ab\ initio}$) for both analytical PESs: (a) $^2A'$ (1245 points) and (b) $^4A'$ (910 points).

We have used as a reference structure for the doublet surface a C_{2v} structure which is an average of the CASSCF (17,12) geometries for the two equivalent TS1 (Ref. 15) and the CASSCF(17, 12) geometry of the $NO_2(^2A_1)$ minimum (Ref. 15) (Table I).

The optimal 72 three-body parameters (c_{ijk} and γ_i) are shown in Table I. The final RMSD for the doublet surface was 1.06 kcal/mol for the C_s-abstraction and insertion regions, and 4.86 kcal/mol for the C_{2v}-insertion region. The global RMSD for this surface was 2.82 kcal/mol. Figure 2 shows the energy deviations (i.e., $\Delta E_{fit} = E_{analytical} - E_{ab\ initio}$) of the fit with a very narrow distribution. Despite of the RMSD, the C_{2v} region could seem relatively high, it should

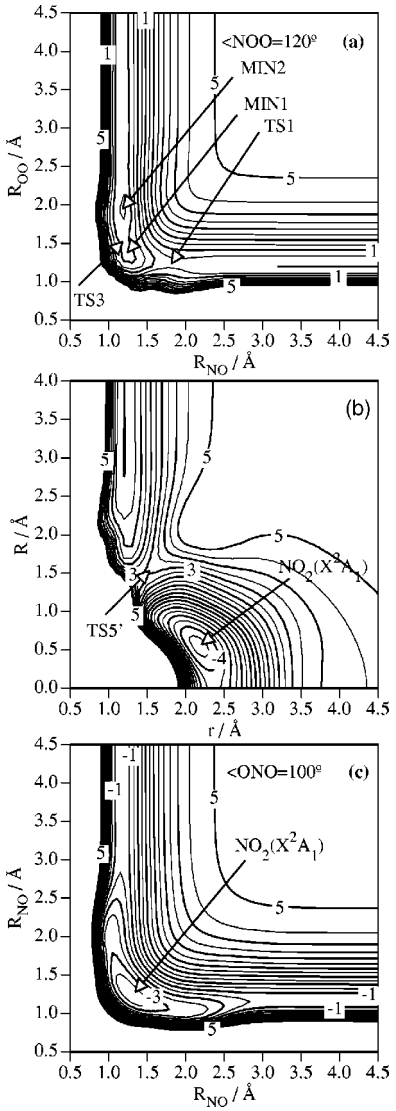

FIG. 3. Equipotential contour diagrams of the $^2A'$ analytical PES for C_s and C_{2v} geometries. The contours are depicted in increments of 0.5 eV and the zero of energy is taken in reactants [i.e., $N(^4S)+O_2$].

be taken into account that the energetic difference between the highest (i.e., transition state for the C_{2v} insertion) and the lowest (i.e., NO_2 molecule) of the stationary points is very large, around 179 kcal/mol. On the other hand, as it was concluded in Paper II in base to the energetics, the C_{2v}-insertion mechanism will not be important compared with the C_s-abstraction and insertion mechanisms even at very high temperatures. Therefore, an optimal fit of the C_s-NOO regions is much more essential for the study of this reaction and also for its reverse.

Figure 3 presents some equipotential energy curves corresponding to the $^2A'$ PES, where it is possible to see the different stationary points fitted for C_s [Fig. 3(a)] and C_{2v} [Figs. 3(b) and 3(c)] geometries. The properties of the stationary points for this PES are depicted in Table III. In general there is a good agreement between the *ab initio* properties reported in Papers I and II and the analytical properties of these stationary points, especially for the two most important (i.e., TS1 and NO_2 molecule). Only an extra van der Waals minimum type is found here (MIN*A*), placed 1.82 kcal/mol below the $O(^3P)+NO$ products. Several IRC calculations were carried out to make sure the connections that are shown in Fig. 4(a). We have also verified that MIN1 connects directly with products $O(^3P)+NO(X\,^2\Pi)$ increasing the NOO angle, but the *ab initio* TS2 responsible for this connection could not be fitted. As it was shown in Paper I, this saddle point has an energy very close to that for MIN1, that is, this region is too flat, and because of this the accuracy of the fit becomes extremely demanding.

C. $^4A'$ analytical PES

A similar procedure as for the $^2A'$ analytical PES has been followed for the $^4A'$ analytical PES. Both PESs use the same diatomic curves and therefore reproduce the same experimental exoergicity. As reference structure it was taken as an average of the geometries for two CASSCF(17, 12) C_{2v} stationary points [i.e., TS2($^4A_1$) and MIN1($^4B_2$) (Ref. 16)] along with an average between both equivalent CASSCF(17,

TABLE III. Properties of the several stationary points located on the $^2A'$ analytical PES.

C_s sym.	$R_{e(NO)}$/Å	$R_{e(OO)}$/Å	<NOO/°	ω_i/cm^{-1} [a]			ΔE/kcal mol^{-1} [b]
TS1	1.9012	1.2337	109.06	485.81*i*	399.02	1221.05	6.87 (6.90)
TS3	1.2020	1.4757	125.81	1438.45	474.40	542.46*i*	−27.42 (−26.97)
TS4	1.1512	2.0071	88.40	1350.65	398.40*i*	287.08	−34.26 (−34.20)
MIN1	1.2410	1.3381	121.71	1317.39	437.50	855.93	−28.50 (−27.05)
MIN2	1.1681	1.9661	116.98	1792.60	443.44	299.49	−37.64 (−36.30)
MIN A	1.1557	2.6834	180.00	1918.46	32.50(2)	130.84	−1.82 (−1.52)[c]

C_{2v} sym.	R_e(NO)/Å	<ONO/°	ω_i/cm^{-1} [a]			ΔE/kcal mol^{-1} [b]
NO_2	1.2183	125.91	995.53	668.91	1384.90	−108.68 (−106.60)
TS5′	1.6524	52.79	1388.98*i*	835.72	974.75*i*	69.98 (68.89)

[a]Harmonic vibrational frequencies (a) for the C_s geometries ω_1 (NO str., a'), ω_2 (NOO bend., a'), and ω_3 (OO str., a'), respectively, and (b) for the C_{2v} geometries ω_s (sym. str., a_1), ω_b (bend., a_1), and ω_a (asym. str., b_2), respectively (*YZ* taken as the molecular plane). Masses of the most abundant isotopes were used: ^{14}N and ^{16}O.

[b]Energy barrier respect to $N(^4S)+O_2$. The value corrected with the difference of zero point energies is shown in parentheses.

[c]Referred to $O(^3P)+NO$.

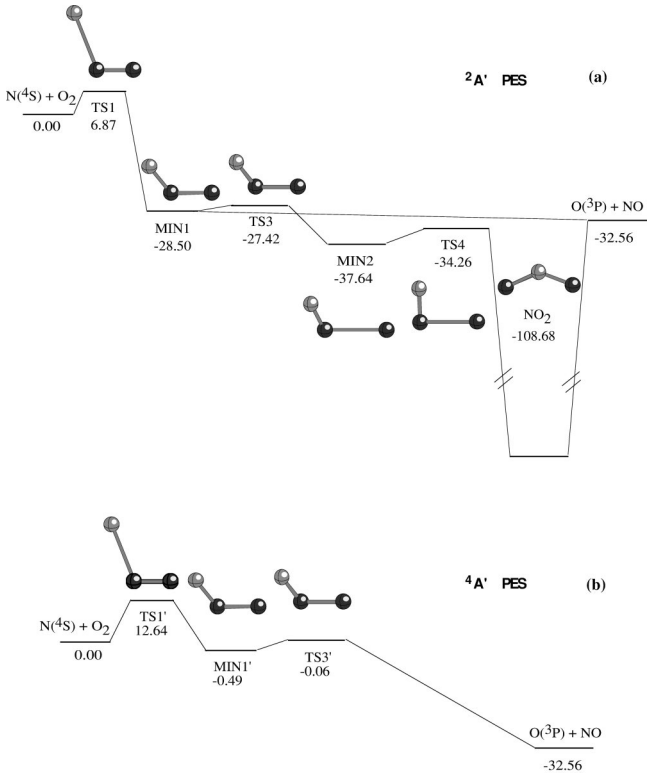

FIG. 4. Schematic representation of the lowest MEP for both the $^2A'$ (a) and the $^4A'$ (b) analytical PESs. Energies are given relative to reactants, $N(^4S)+O_2$, in kcal/mol.

12) TS1′($^4A'$) geometries.[15] This reference structure was however very similar to that derived for the $^2A'$ surface (Table I).

Approximately 910 *ab initio* points [CASPT2 (17, 12) G2/aug-cc-pVTZ] have been calculated in different regions of the $^4A'$ PES to be used in the analytical fit, as it is summarized below: (a) 442 points for the $N(^4S)+O_2-C_s$-abstraction mechanism: 313 points at different NOO angles (90°, 120°, 150° and 180°) for 1.05 Å$\leqslant R_{NO}\leqslant$4.5 Å and 1.1 Å$\leqslant R_{OO}\leqslant$4.5 Å and 129 points around the stationary points TS1′, TS3′, and MIN1′ (Ref. 15) (bending and stretching distortions), (b) 461 points for the $N(^4S)+O_2-C_{2v}$-insertion mechanism for 0.0 Å$\leqslant R\leqslant$5.0 Å and 1.1 Å$\leqslant r\leqslant$2.6 Å, mainly around the TS2($^4A_1$) and MIN1($^4B_2$) stationary points.[16] For this surface it was necessary to use some weights throughout the fit: (1) 1.0 for all *ab initio* points, (2) 10.0 for a grid of O+NO points with C_s symmetry (40 points) and C_{2v} symmetry (68 points), and (3) 20.0 for a different set of O+NO points with C_s symmetry (56 points). Moreover, the energies and first-order partial derivatives of TS1′, TS3′, and MIN1′ were also fitted, together with the second-order partial derivatives for TS1′, all with a weight of 1.0. The same shift for the energies of the *ab initio* points in the entrance channel aforementioned for the doublet fit was also introduced for the quartet fit. Finally we decided to use the corresponding *ab initio* energy barrier of TS1′ as scarce experimental information was available to scale that, and on the other hand, the *ab initio* value was similar in comparison to different *ab initio* and DFT results.[15]

The final RMSD for the quartet surface was 1.67 kcal/mol for the C_s-abstraction region and 2.46 kcal/mol for the C_{2v}-insertion region. The global RMSD for this surface was 2.12 kcal/mol (Fig. 2). Figure 5 shows some equipotential curves corresponding to the $^4A'$ PES, where it is possible to see several stationary points fitted for C_s [Fig. 5(a)] and C_{2v} [Figs. 5(b) and 5(c)] geometries. The properties of the different stationary points are depicted in Table IV, and Fig. 4(b) presents a MEP for the C_s-abstraction mechanism. Apart from the *ab initio* stationary points, two additional van der Waals minima have been found, one in the entrance channel (MIN *B*) of −1.75 kcal/mol [referred to $N(^4S)+O_2$] and another in the exit channel (MIN *C*) of −2.51 kcal/mol [referred to $O(^3P)+NO$], even though a small influence can be expected in the kinetics and dynamics of this exoergic reaction.

III. VARIATIONAL TRANSITION STATE THERMAL RATE CONSTANTS

Thermal rate constants for reaction $N(^4S)+O_2(X\,^3\Sigma_g^-)$ and also for its reverse reaction have been calculated within the 300–5000 K temperature range at different levels of the conventional (TST) or variational (VTST) transition state theories as implemented in the POLYRATE program.[43] The rate constant values have been obtained for the following levels of TST and VTST, including or not a semiclassical tunneling correction: TST, TST/μOMT, CVT, CVT/μOMT, ICVT, and ICVT/μOMT. The acronyms CVT, ICVT, and μOMT correspond, respectively, to the canonical VTST, improved canonical VTST, and microcanonical optimized multidimensional tunneling correction. The ICVT/μOMT method is the highest calculation level considered here and its values will be presented in this work and compared with previous published results. Tables V and VI show these values in comparison with experimental data.

From the correlation between reactants and products electronic states and neglecting the possibility of a nonadiabatic coupling between the $^2A'$ and $^4A'$ PESs due to the spin–orbit interaction, the rate constants for the $N(^4S)+O_2(X\,^3\Sigma_g^-)$ reaction can be calculated by

$$k_1=k_1(^2A')+k_1(^4A')=1/6k'_1(^2A')+1/3k'_1(^4A'), \tag{8}$$

where $k_1(^2A')$ and $k_1(^4A')$ include the relative weight of the different PESs, which arise purely from the corresponding electronic degeneracy factors (i.e., 2/12 and 4/12, respectively). The contribution of the $^6A'$ PES has been taken as being equal to zero, since it correlates with products through an electronic excited state not available at the energies involved in the temperature range studied.

To check even more both analytical PESs, rate constants for the reverse reaction have been also computed. In this case, we have introduced a commonly used spin–orbit correction[39] through the reactants electronic partition function (Q) in the calculated rate constants

$$Q^{\mathrm{elec}}_{O(^3P)}(T)=g(^3P_2)+g(^3P_1)e^{-\Delta_1/RT}+g(^3P_0)e^{-\Delta_0/RT}, \tag{9}$$

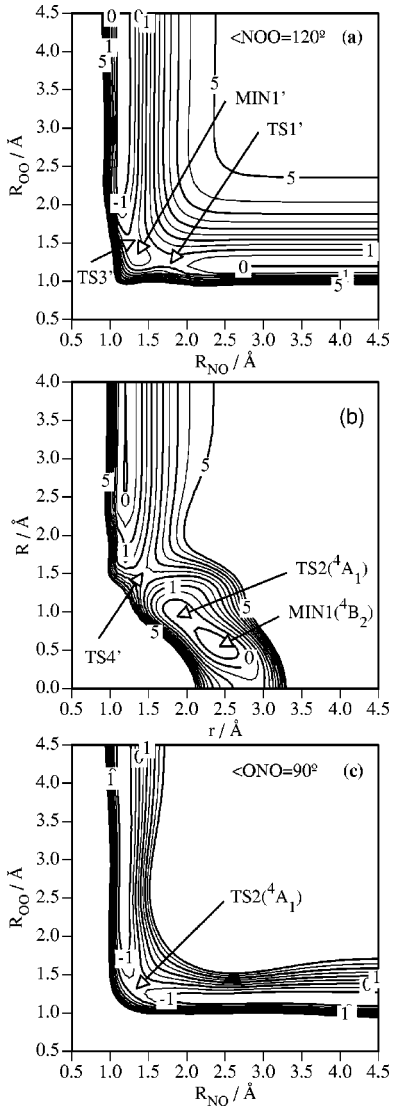

FIG. 5. Equipotential contour diagrams of the $^4A'$ analytical PES for C_s and C_{2v} geometries. The contours are depicted in increments of 0.5 eV and the zero of energy is taken in reactants [i.e., $N(^4S)+O_2$].

where g is the electronic degeneracy of the corresponding oxygen state; $g(^3P_2)$, $g(^3P_1)$, and $g(^3P_0)$ are equal to 5, 3, and 1, respectively, and Δ_i are the energetic differences between the electronic states [$\Delta_1(^3P_1-^3P_2)$ and $\Delta_2(^3P_0-^3P_2)$ are equal to 158.27 and 226.98 cm^{-1}, respectively[1]]. Similarly, for $NO(^2\Pi)$:

$$Q^{elec}_{NO(^2\Pi)}(T)=g(^2\Pi_{1/2})+g(^2\Pi_{3/2})e^{-\Delta_3/RT}, \tag{10}$$

where $g(^2\Pi_{1/2})$ and $g(^2\Pi_{3/2})$ are both equal to 2, and $\Delta_3(^2\Pi_{3/2}-^2\Pi_{1/2})$ is equal to 121.1 cm^{-1}.[1] Thus the expression for k_{-1} can be obtained from

$$k_{-1}=k_{-1}(^2A')+k_{-1}(^4A')$$

$$=\frac{2k'_{-1}(^2A')+4k'_{-1}(^4A')}{(5+3e^{-227.7/T}+e^{-326.6/T})(2+2e^{-174.2/T})}, \tag{11}$$

although at very high temperatures it becomes

$$k_{-1}=\tfrac{1}{18}\ k'_{-1}(^2A')+\tfrac{1}{9}\ k'_{-1}(^4A'). \tag{12}$$

The calculated rate constants conform to the standard three-parameter equation

$$k=AT^n e^{B/T}, \tag{13}$$

where A, n, and B are parameters optimized by means of a least-squares procedure. Their values for both reaction rate constants are given in Figs. 5 and 6.

The rate constants for the direct reaction on the $^2A'$ analytical PES are much larger than the ones for the $^4A'$ analytical PES, with the exception of what happens at very high temperatures. At 1000, 2000, and 3000 K, $k_1(^2A')/k_1(^4A')$ is equal to 10.2, 2.3, and 1.4, respectively; at the highest temperature considered (i.e., 5000 K) this value becomes 0.96, which represents the major contribution (i.e., 51.1%) of $k(^4A')$ to the total rate constant.

The new values for $k_1(^2A')$ are lower than the previous ones[17] (Table V) under 1000 K but the behavior is opposite over this temperature. In spite of the energy barrier for the new analytical PES is a bit higher than for the previous one, which would produce lower rate constants with the new PES, the vibrational partition function of the transition state in-

TABLE IV. Properties of several stationary points located on the $^4A'$ analytical PES.

C_s sym.	$R_{e(NO)}$/Å	$R_{e(OO)}$/Å	<NOO/°	ω_i/cm^{-1} [a]			ΔE/kcal mol^{-1} [b]
TS1′	1.8295	1.2419	100.57	563.46*i*	379.66	1359.49	12.64(12.85)
TS3′	1.2899	1.4672	109.37	1379.43	463.36	463.72*i*	−0.06(0.29)
MIN1′	1.3493	1.3505	110.22	1180.28	494.40	680.43	−0.49(0.60)
MIN B	2.7987	1.1938	77.72	171.39	138.62	1597.60	−1.75(−1.30)
MIN C	1.1529	3.2084	180.00	1925.79	44.17(2)	129.95	−2.51(−2.16)[c]

C_{2v} sym.	$R_{e(NO)}$/Å	ONO/°	ω_i/cm^{-1} [a]			ΔE/kcal mol^{-1} [b]
MIN1	1.3268	129.65	1153.00	570.13	540.26	−20.23(−19.27)
TS2	1.3459	93.41	1095.87	43.08	596.58*i*	−9.74(−10.39)
TS4′	1.6551	51.34	1129.55*i*	998.35	806.08*i*	54.87(54.02)

[a]Harmonic vibrational frequencies (a) for the C_{2v} geometries ω_1 (NO str., a'), ω_2 (NOO bend., a'), and ω_3 (OO str., a'), respectively, and (b) for the C_{2v} geometries ω_s (sym. str., a_1), ω_b (bend., a_1), and ω_a (asym. str., b_2), respectively (*YZ* taken as the molecular plane). Masses of the most abundant isotopes were used ^{14}N and ^{16}O.

[b]Energy barrier respect to $N(^4S)+O_2$. The value corrected with the difference of zero point energies is shown in parentheses.

[c]Referred to $O(^3P)+NO$.

TABLE V. Theoretical ICVT/μOMT and experimental thermal rate constants for the $N(^4S)+O_2(X\,^3\Sigma_g^-)\rightarrow O(^3P)+NO(X\,^2\Pi)$ reaction.[a]

	$k_1(^2A')$		$k_1(^4A')$		k_1 [b]		
T/K	This work	Previous work[c]	This work	Previous work[d]	This work	Previous work[c,d]	Experiment[e]
300	7.64×10^{-17}	8.67×10^{-17}	7.77×10^{-21}	9.50×10^{-23}	7.64×10^{-17}	8.67×10^{-17}	8.31×10^{-17}
600	2.97×10^{-14}	3.22×10^{-14}	4.10×10^{-16}	4.64×10^{-17}	3.01×10^{-14}	3.22×10^{-14}	3.87×10^{-14}
1000	4.27×10^{-13}	4.22×10^{-13}	4.20×10^{-14}	1.10×10^{-14}	4.69×10^{-13}	4.34×10^{-13}	5.72×10^{-13}
1500	1.90×10^{-12}	1.75×10^{-12}	5.00×10^{-13}	1.98×10^{-13}	2.41×10^{-12}	1.95×10^{-12}	2.54×10^{-12}
2000	4.38×10^{-12}	3.83×10^{-12}	1.88×10^{-12}	0.91×10^{-12}	6.27×10^{-12}	4.75×10^{-12}	5.85×10^{-12}
3000	1.13×10^{-11}	0.93×10^{-11}	7.93×10^{-12}	4.67×10^{-12}	1.92×10^{-11}	1.40×10^{-11}	1.51×10^{-11}
4000	1.95×10^{-11}	1.55×10^{-11}	1.75×10^{-11}	1.15×10^{-11}	3.70×10^{-11}	2.70×10^{-11}	2.65×10^{-11}
5000	2.82×10^{-11}	2.20×10^{-11}	2.95×10^{-11}	2.05×10^{-11}	5.77×10^{-11}	4.25×10^{-11}	3.90×10^{-11}

[a]Rate constants are given in $cm^3\,molecule^{-1}\,s^{-1}$.
[b]The theoretical total rate constant k_1 is calculated using Eq. (8).
[c]Reference 17.
[d]Reference 18.
[e]Reference 7. $\Delta \log k_1=\pm0.12$ over the range 298–1000 K rising to ±0.3 over the range 1000–5000 K.

creases much more with the raise of the temperature for the new $^2A'$ analytical PES than for the old one, explaining that at higher temperatures than 1000 K $k_1(^2A',\text{new}) > k_1(^2A',\text{old})$.

The present results show more contribution of the excited $^4A'$ PES to the total rate constant (k_1) for the complete range of temperatures in comparison to the previous results,[17] mainly due to the minor energy barrier (i.e., 12.64 kcal/mol) compared with the corresponding previous $^4A'$ PES value (i.e., 15.0 kcal/mol[18]). The agreement between the calculated rate constants and the experimental data is very good (see Table V or Fig. 6), within the experimental error bars. In spite of the present, results are very close to the latest ones,[17] there is an important difference as all previous $^2A'$ PES did not reproduced properly the NO_2 ($X\,^2A_1$) minimum and it seems to have an important dynamic effect on this reaction,[28] though no kinetics. In fact, our preliminary QCT studies show that an important percentage of the trajectories explore this region of the PES. Nevertheless, a small influence on the calculated rate constants can be expected as the key kinetic factor seems to be the value of the energy barrier at the reactant region of the PES [see the MEP in Fig. 4(a)]: preliminary QCT rate constants are very close to VTST values [e.g., $k_1=1.43\times10^{-15}$(QCT) versus 1.40×10^{-15}(VTST) $cm^3\,molecule^{-1}\,s^{-1}$ at 400 K].

Despite the reaction in this study involve heavy atoms, the transmission coefficients κ calculated by means of the μOMT method at different temperatures are high even at room temperature (e.g., 1.27 for $^2A'$ and 1.38 for the $^4A'$ at 300 K) as it was also found in the previous study.[17]

A similar behavior was obtained for the reverse reaction (see Table VI and Fig. 7). For both reactions the TST or VTST rate constants are quite similar to each other. Moreover, the different methods used to determine the tunneling correction gave place to similar values.

IV. CONCLUSIONS AND REMARKS

In this work we have derived analytical fits of the ground PES ($^2A'$) and the first excited PES ($^4A'$) involved into the $N(^4S)+O_2(X\,^3\Sigma_g^-)\rightarrow O(^3P)+NO(X\,^2\Pi)$ reaction and its reverse, using *ab initio* data reported in Papers I and II along with new grids of *ab initio* points [CASPT2 (17,12) G2/aug-cc-pVTZ calculations] reported here. Some experimental data was also introduced to better account for the exoergicity and the experimental rate constant at 300 K. The final RMSD

TABLE VI. Theoretical ICVT/μOMT and experimental thermal rate constants for the $O(^3P)+NO(X\,^2\Pi)\rightarrow N(^4S)+O_2(X\,^3\Sigma_g^-)$ reaction.[a]

	$k_1(^2A')$		$k_1(^4A')$		k_1 [b]		
T/K	This work	Previous work[c]	This work	Previous work[d]	This work	Previous work[c,d]	Experiment[e]
300	1.31×10^{-40}	2.58×10^{-40}	1.33×10^{-44}	2.82×10^{-46}	1.31×10^{-40}	2.58×10^{-40}	
600	2.38×10^{-26}	3.42×10^{-26}	3.27×10^{-28}	4.90×10^{-29}	2.42×10^{-26}	3.42×10^{-26}	
1000	1.60×10^{-20}	1.90×10^{-20}	1.58×10^{-21}	4.96×10^{-22}	1.76×10^{-20}	1.95×10^{-20}	1.28×10^{-20}
1500	1.56×10^{-17}	1.65×10^{-17}	4.13×10^{-18}	1.86×10^{-18}	1.98×10^{-17}	1.83×10^{-17}	1.22×10^{-17}
2000	5.35×10^{-16}	5.22×10^{-16}	2.30×10^{-16}	1.23×10^{-16}	7.65×10^{-16}	6.45×10^{-16}	4.15×10^{-16}
3000	2.05×10^{-14}	1.84×10^{-14}	1.44×10^{-14}	9.24×10^{-15}	3.49×10^{-14}	2.77×10^{-14}	1.61×10^{-14}
4000	1.37×10^{-13}	1.18×10^{-13}	1.23×10^{-13}	8.68×10^{-14}	2.60×10^{-13}	2.04×10^{-13}	1.10×10^{-13}
5000	4.46×10^{-13}	3.73×10^{-13}	4.68×10^{-13}	3.48×10^{-13}	9.14×10^{-13}	7.21×10^{-13}	3.71×10^{-13}

[a]Rate constants are given in $cm^3\,molecule^{-1}\,s^{-1}$.
[b]The theoretical total rate constant k_{-1} is calculated according to Eq. (11). $k_{-1}(^2A')$ and $k_{-1}(^4A')$ are obtained by using only the corresponding electronic statistical factors 1/18 and 1/9, respectively, to facilitate the comparison with previous results.
[c]Reference 17.
[d]Reference 18.
[e]Reference 7. $\Delta \log k_{-1}=\pm0.3$.

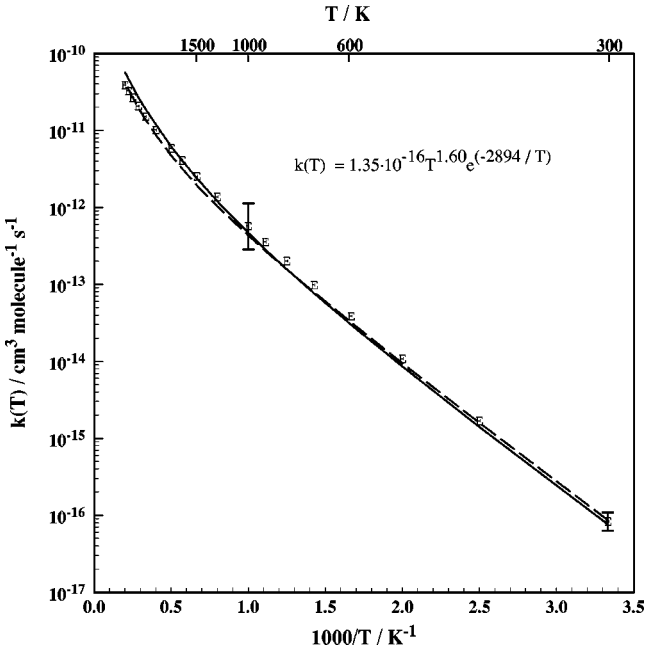

FIG. 6. Arrhenius plots of the calculated and experimental thermal rate constants (300–5000 K) for the $N(^4S)+O_2(X\,^3\Sigma_g^-)\rightarrow O(^3P)+NO(X\,^2\Pi)$ reaction:(—) ICVT/μOMT values with the new analytical PESs, (---) ICVT/μOMT values with the old PESs (Refs. 17 and 18), and (○) experimental data (Ref. 7) with one typical error bar. The *A*, *n*, and *B* optimal parameters for the fit [Eq. (13)] of the present calculated rate constants are also indicated.

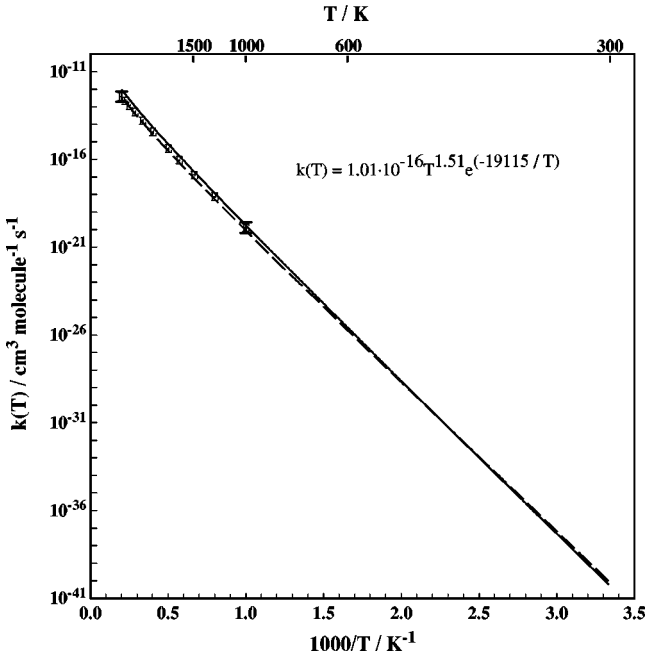

FIG. 7. Arrhenius plots of the calculated and experimental thermal rate constants (300–5000 K) for the $O(^3P)+NO(X\,^2\Pi)\rightarrow N(^4S)+O_2(X\,^3\Sigma_g^-)$ reaction:(—) ICVT/μOMT values with the new analytical PESs, (---) ICVT/μOMT values with the old PESs (Refs. 17 and 18), and (○) experimental data (Ref. 7) with one typical error bar. The *A*, *n*, and *B* optimal parameters for the fit [Eq. (13)] of the present calculated rate constants are also indicated.

for the doublet surface was 1.06 kcal/mol for the C_s-abstraction and insertion regions, 4.86 kcal/mol for the C_{2v}-insertion region (2.82 kcal/mol for all PES), and for the quartet surface was 1.67 kcal/mol for the C_s-abstraction region, 2.46 kcal/mol for the C_{2v}-insertion region (2.12 kcal/mol for all PES).

Thermal rate constants were calculated for both the direct and the reverse reactions by means of the variational transition state theory with the inclusion of a microcanonical optimized multidimensional tunneling correction. The theoretical values are in good agreement with experimental measurements even at very high temperatures. In spite that the new PESs give place to similar kinetic results as in our previous studies, the expected dynamical behavior could be rather different. The new $^2A'$ analytical PES describes properly the NO_2 $(X\,^2A_1)$ minimum, which seem to be very accessible in the trajectories run in our preliminary QCT study, and other stationary points not introduced in previous analytical PESs.

The new analytical $^4A'$ PES has a lower energy barrier than the previous one, which increases significantly the contribution of this PES to the total rate constant at high temperatures. Additional theoretical and experimental studies could help to refine much more the value of the main energy barrier.

On the other hand, the new PESs not only accurately describe the C_s regions of the NOO system but also the ONO C_{2v} or near C_{2v} regions. Previous analytical PESs were based on extremely limited *ab initio* information. Both PESs can be used to study the $N(^4S)+O_2(X\,^3\Sigma_g^-)\rightarrow O(^3P)+NO(X\,^2\Pi)$ reaction and its reverse one, and also can be useful to study the oxygen exchange reaction: $O(^3P)+NO'(X\,^2\Pi)\rightarrow O'(^3P)+NO(X\,^2\Pi)$, without an energy barrier for the $^2A'$ surface and with an energy barrier of 22.82 kcal/mol for the $^4A'$ surface.

A dynamical study (e.g., using the QCT method or quantum dynamics wave packet approach) will be able to ascertain the extension of the different microscopic mechanisms proposed in Papers I and II for this reaction: (a) direct near C_{2v}-insertion mechanism, (b) direct C_s-abstraction mechanism, and (c) indirect C_s-insertion mechanism. A QCT study on both PESs is in progress at present in our research group to see the importance of several microscopic mechanisms and the corresponding contribution of each PES to the global behavior. This dynamics study will also allow us to elucidate the importance of the peroxy $NOO(^2A')$ and the $NO_2(X\,^2A_1)$ minima, not well described in preceding doublet analytical PESs.

ACKNOWLEDGMENTS

This work has been supported by the ''Dirección General de Enseñanza Superior (Programa Sectorial de Promoción General del Conocimiento)'' of the Spanish Ministry of Education and Culture (DGES Project Ref. PB 98-1209-C02-01). Financial support from the European Union (INTAS Project Ref. 99-00701) and the ''Generalitat'' (Autonomous Government) of Catalonia (Projects Refs. 1998SGR 0008 and 2000SGR 00016) is also acknowledged. C.O. thanks the Spanish Ministry of Education and Culture for a predoctoral research grant. The authors are grateful to the

"Centre de Computació i Comunicacions de Catalunya (C^4–CESCA/CEPBA)" for providing a part of the computer time.

[1] M. W. Chase, Jr., C. A. Davies, J. R. Downey, Jr., D. J. Frurip, R. A. McDonald, and A. N. Syverud, J. Phys. Chem. Ref. Data **14**, 1 (1985).
[2] P. Warneck, in *Chemistry of the Natural Atmosphere* (Academic, San Diego, 1998), Chap. 3.
[3] V. I. Shematovich, D. V. Bisikalo, and J. C. Gérard, Geophys. Res. Lett. **18**, 1691 (1991).
[4] A. Burcat, G. Dixon-Lewis, M. Frenklach, W. C. Gardiner, R. K. Hanson, S. Salimian, J. Troe, J. Warnatz, and R. Zellner, in *Combustion Chemistry*, edited by W. C. Gardiner, Jr. (Springer-Verlag, New York, 1984).
[5] N. Balakrishnan, E. Sergueeva, V. Kharchenko, and A. Dalgarno, J. Geophys. Res. **105**, 18549 (2000).
[6] W. B. DeMore, D. M. Golden, R. F. Hampson, M. J. Kurylo, C. J. Howard, A. R. Ravishankara, C. E. Kolb, and M. J. Molina, in *Chemical Kinetics and Photochemical Data for Use in Stratospheric Modelling*, Evaluation 12, JPL Publ. 97-4 (Jet Propulsion Laboratory, Pasadena, CA, 1997).
[7] D. L. Baulch, C. J. Cobos, R. A. Cox *et al.*, J. Phys. Chem. Ref. Data **23**, 847 (1994).
[8] M. E. Whitson, Jr., L. A. Darnton, and R. J. McNeal, Chem. Phys. Lett. **41**, 552 (1976).
[9] A. Rahbee and J. J. Gibson, J. Chem. Phys. **74**, 5143 (1981).
[10] R. R. Herm, B. J. Sullivan, and M. E. Whitson, Jr., J. Chem. Phys. **79**, 2221 (1983).
[11] I. C. Winkler, R. A. Stachnik, J. I. Steinfeld, and S. M. Miller, J. Chem. Phys. **85**, 890 (1986).
[12] G. E. Caledonia, R. H. Krech, D. B. Oakes, S. J. Lipson, and W. A. M. Blumberg, J. Geophys. Res. **105**, 12833 (2000).
[13] S. P. Walch and R. L. Jaffe, J. Chem. Phys. **86**, 6946 (1987), and references therein. Also see AIP Document No. PAPSJCPSA-86-6946-10.
[14] G. Suzzi Valli, R. Orrú, E. Clementi, A. Laganà, and S. Crocchianti, J. Chem. Phys. **102**, 2825 (1995).
[15] R. Sayós, C. Oliva, and M. González, J. Chem. Phys. **115**, 1287 (2001).
[16] M. González, C. Oliva, and R. Sayós, J. Chem. Phys. **117**, 680 (2002), following paper.
[17] R. Sayós, J. Hijazo, M. Gilibert, and M. González, Chem. Phys. Lett. **284**, 101 (1998).
[18] J. W. Duff, F. Bien, and D. E. Paulsen, Geophys. Res. Lett. **21**, 2043 (1994).
[19] M. Gilibert, A. Aguilar, M. González, and R. Sayós, Chem. Phys. **172**, 99 (1993).
[20] A. J. C. Varandas and A. I. Voronin, Mol. Phys. **85**, 497 (1995).
[21] R. L. Jaffe, M. D. Pattengill, and D. W. Schwenke, in *Supercomputer Algorithms for Reactivity, Dynamics and Kinetics of Small Molecules*, edited by A. Laganà (Kluwer, Dordrecht, 1989), p. 367.
[22] M. Gilibert, A. Aguilar, M. González, and R. Sayós, Chem. Phys. **178**, 178 (1993).
[23] R. Sayós, A. Aguilar, M. Gilibert, and M. González, J. Chem. Soc., Faraday Trans. **89**, 3223 (1993).
[24] D. Bose and G. V. Candler, J. Chem. Phys. **107**, 6136 (1997).
[25] B. Ramachandran, N. Balakrishnan, and A. Dalgarno, Chem. Phys. Lett. **332**, 562 (2000).
[26] M. Gilibert, X. Giménez, M. González, R. Sayós, and A. Aguilar, Chem. Phys. **191**, 1 (1995).
[27] N. Balakrishnan and A. Dalgarno, Chem. Phys. Lett. **302**, 485 (1999).
[28] P. Defazio, C. Petrongolo, S. K. Gray, and C. Oliva, J. Chem. Phys. **115**, 3208 (2001).
[29] B. O. Roos, P. R. Taylor, and P. E. M. Siegbahn, Chem. Phys. **48**, 157 (1980).
[30] B. O. Roos, in *Advances in Chemical Physics: Ab Initio Methods in Quantum Chemistry-II*, edited by K. P. Lawley (Wiley, Chichester, 1987), Vol. LXIX, p. 399.
[31] M. W. Schmidt and M. S. Gordon, Annu. Rev. Phys. Chem. **49**, 233 (1998).
[32] T. H. Dunning, Jr., J. Chem. Phys. **90**, 1007 (1989).
[33] K. Andersson, P.-Å. Malmqvist, and B. O. Roos, J. Chem. Phys. **96**, 1218 (1992).
[34] K. Andersson, M. R. A. Blomberg, M. P. Fülscher *et al.*, Lund University (Sweden) 1998, MOLCAS 4.1 program.
[35] J. N. Murrell, S. Carter, S. C. Farantos, P. Huxley, and A. J. C. Varandas, *Molecular Potential Energy Surfaces* (Wiley, New York, 1984).
[36] M. González and R. Sayós, DIATOMFIT (unpublished).
[37] R. Sayós and M. González, SM3FIT (unpublished).
[38] M. González, I. Miquel, and R. Sayós, J. Chem. Phys. **115**, 2530 (2001).
[39] M. González, R. Valero, and R. Sayós, J. Chem. Phys. **113**, 10983 (2000).
[40] R. Sayós, J. Hernando, J. Hijazo, and M. González, Phys. Chem. Chem. Phys. **1**, 947 (1999).
[41] K. P. Huber and G. Herzberg, *Molecular Spectra and Molecular Structure IV. Constants of Diatomic Molecules* (Van Nostrand–Reinhold, New York, 1979).
[42] D. G. Truhlar, B. C. Garrett, and S. J. Klippenstein, J. Phys. Chem. **100**, 12771 (1996).
[43] R. Steckler, Y. Chuang, E. L. Coitiño *et al.*, Department of Chemistry and Supercomputer Institute, University of Minnesota, Minneapolis, MN 55455, POLYRATE, version 7.0, 1996.